ISPRS Journal of Photogrammetry and Remote Sensing 66 (2011) 347–355

Contents lists available at ScienceDirect

ISPRS Journal of Photogrammetry and Remote Sensing

journal homepage: www.elsevier.com/locate/isprsjprs

Epipolar resampling of linear pushbroom satellite imagery by a new epipolarity model☆

Mi Wang[a,*], Fen Hu[b], Jonathan Li[c]

[a] Liesmars, Wuhan University, No. 129, Luoyu Road Wuhan, Hubei 430079, China

[b] Satellite Surveying and Mapping Application Center, State Bureau of Surveying and Mapping, Beijing, 100830, China

[c] University of Waterloo, Ontario, Canada

ARTICLE INFO

Article history:
Received 5 April 2010
Received in revised form
25 December 2010
Accepted 3 January 2011
Available online 5 February 2011

Keywords:
Photogrammetry
Epipolar resampling
Linear pushbroom satellite imagery

ABSTRACT

This paper presents a practical epipolarity model for high-resolution linear pushbroom satellite images acquired in either along-track or cross-track mode, based on the projection reference plane in object space. A new method for epipolar resampling of satellite stereo imagery based on this model is then developed. In this method, the pixel-to-pixel relationship between the original image and the generated epipolar image is established directly by the geometric sensor model. The approximate epipolar images are generated in a manner similar to digital image rectification. In addition, by arranging the approximate epipolar lines on the defined projection reference plane, a stereoscopic model with consistent ground sampling distance and parallel to the object space is thus available, which is more convenient for three-dimensional measurement and interpretation. The results obtained from SPOT5, IKONOS, IRS-P5, and QuickBird stereo images indicate that the generated epipolar images all achieve high accuracy. Moreover, the vertical parallaxes at check points are at sub-pixel level, thus proving the feasibility, correctness, and applicability of the method.

1. Introduction

Epipolar resampling aims to generate rectified images so that the stereo disparities are parallel to one of the image axes, thus providing advantageous conditions for automatic image matching, digital elevation model (DEM) generation, and stereo measurement (Cochran, 1995; Ono et al., 1999; Hashimoto, 2000; Bang et al., 2003; Lee et al., 2003; Morgan, 2004; Kornus et al., 2006). As is well known, epipolar resampling is a well-established procedure for images captured by a frame camera (Zhang, 1998; Torr, 2002), as the rigorous epipolar geometry can be easily defined and the epipolar lines are in a simple, straightforward linear style. However, as the leading payload of high-resolution imaging satellites, linear array pushbroom scanners are characterized by their particularly distinct imaging principle and their diverse, complex physical structures in comparison with conventional frame cameras. That is, the image scenes are formed by stitching the one-dimensional (1D) scan lines captured as the sensor moves (Wolf and Dewitt, 2000). On the one hand, it is almost impossible to rigorously define the epipolar geometry of linear pushbroom satellite imagery, primarily because the determination of the accurate geometric relationship between object space and image space (i.e., sensor modeling) is difficult due to the adopted multi-center projection imaging mode. On the other hand, the resulting epipolar lines are actually not straight lines on the original image scenes, which brings complexity and difficulty to epipolar resampling. As a result, for satellite stereo imagery, the classical epipolar theory and methodology applied to single perspective frame-based imagery will no longer be feasible. Actually, epipolar resampling is the arrangement of epipolar lines based on a specific epipolarity model, so it is theoretically and practically significant to study the epipolarity model of linear pushbroom satellite stereo imagery.

In general, the existing epipolarity models can be categorized into two classes: (1) the models for finding epipolar curves in image space by image correspondence, and (2) the models for exploiting epipolar geometry based on a geometric sensor model. In the first category, the most often used model is the polynomial fit model (PFM), which was proposed and discussed to arrange the approximate epipolar curves of the SPOT cross-track stereo imagery in the late 1980s (Su, 2002). In the second category,

☆ A new method for generating approximate epipolar images from high-resolution linear pushbroom satellite stereo images based on the projection reference plane in object space.

* Corresponding author. Tel.: +86 27 68778969, +86 013971351686; fax: +86 27 68778969.

E-mail addresses: wangmi@lmars.whu.edu.cn (M. Wang), hufen1984@163.com (F. Hu), junli@uwaterloo.ca (J. Li).

0924-2716/$ – see front matter © 2011 International Society for Photogrammetry and Remote Sensing, Inc. (ISPRS). Published by Elsevier B.V. All rights reserved.
doi:10.1016/j.isprsjprs.2011.01.002

the Projection Trajectory based Epipolarity Model (PTEM) and the Parallel Projection transformation based Epipolarity Model (PPEM) are two typical examples. The Projection Trajectory (PT) based epipolar curve definition is most widely known and accepted for linear pushbroom satellite images (Alrousan et al., 1997), and can be extended to conventional frame-based images. Considerable effort has been expended on the PTEM and the major achievement has been the derivation of the mathematical form of the epipolar geometry from the rigorous sensor model based on collinearity equations (Kim, 2000; Bang et al., 2003; Zhao et al., 2008) and the simplified pushbroom sensor model (Lee and Park, 2002). Accordingly, the geometric properties of the theoretically non-straight epipolar lines can thus be visibly analyzed, providing constructive instructions to the epipolarity related applications of linear pushbroom satellite images. In recent years, PPEM has been studied and applied to epipolar resampling of high-resolution linear pushbroom satellite imagery (e.g., IKONOS, QuickBird, etc.) (Morgan et al., 2004a,b, 2006; Jaehong et al., 2006). Due to the small field of view (FOV) of this type of spaceborne linear pushbroom scanner, the perspective projection sensor model of such satellite images is first transformed to a parallel projection sensor model (Fraser and Yamakawa, 2004), and then the epipolar geometry parameters can be determined by at least four pairs of conjugate points, according to the property that the parallel projection stereo imagery holds a unified epipolar line direction. Finally the epipolar images are generated in a manner similar to the process of digital image rectification. The feasibility of PPEM used for epipolar resampling towards automatic DEM generation from high-resolution satellite images has already been investigated (Morgan, 2004; Habib et al., 2004).

Although the existing models described above have been used to generate approximate epipolar images of satellite stereo imagery, technical limitations still exist when the generality, applicability, and simplicity of these models are taken into account. For example, epipolarity models established from either coordinate polynomial fitting or image projection trajectories are without exception in a non-linear style and the derivation of these models needs a certain number of qualified conjugate image points or image orientation parameters, which brings the great complexity to the epipolar resampling process. Moreover, the applicability of PPEM is actually not fully universal because the model needs to work well under the condition that the sensor's FOV is small, and the degree of approximation of the parallel projection model to the perspective projection model relates to topographic conditions and terrain relief, roll angle of the scanner, as well as some other factors. Moreover, compared with the rigorous perspective projection model, although it only requires a small number of parameters to describe the sensor model of parallel projection images holding straight epipolar lines parallel with each other, it needs a certain number of well-matched conjugate image points, along with ground control points (GCPs) and sometimes the roll angle of the imaging sensor to decide the parameters for perspective to parallel projection transformation, as well as epipolar resampling (Morgan et al., 2006; Jaehong et al., 2006). And all of these to a large extent restrict the degree of applicability of the PPEM. Currently, how to produce a qualified epipolar image directly from the provided high-accuracy orientation data of satellite stereo images, especially from the rational polynomial coefficients (RPC) of the rational function model (RFM), is yet an unsolved problem (Zhao et al., 2008) in the application field of high-resolution satellite imagery.

Under these circumstances, our previous work (Hu et al., 2008) initially proposed an epipolarity model of satellite stereo imagery based on the Virtual Horizontal Plane (VHP) in object space. The feasibility of our original idea was validated using only the VHP-based epipolar resampling method to generate the approximate epipolar images of 5 m resolution panchromatic SPOT5-HRG stereo imagery. Therefore, the epipolarity model presented in our previous paper lacked depth and comprehensive analysis and validation. In addition, the concept of Virtual Horizontal Plane (VHP) is not very rigorous and understandable.

In this article, we aim to (1) investigate an epipolarity model for satellite stereo imagery based on the Projection Reference Plane (PRP) in object space, (2) develop a PRP-based method for epipolar resampling of linear pushbroom satellite images, (3) focus on universality of the method, by introducing various kinds of satellite images with different stereoscopic imaging modes and terrain conditions in the experiments, and finally (4) exploit some key factors that affect the accuracy of epipolar resampling results for optional technical routines and better performance of the epipolar resampling method. The newly proposed model needs no sensor model transformation as does PPEM, and needs no conjugate image points or ground control points (GCP) but just orientation data of satellite stereo images to decide the direction for epipolar rearrangement. Overall, the PRP-based method for epipolar resampling is more applicable and universal in practice.

The reminder of the paper is organized as follows. The next section introduces the principle and foundation of our PRP-based epipolarity model by recalling the geometric properties of epipolar curves of linear pushbroom satellite images, along with theoretical reasoning on practical image data. The following sections describe the workflow for generating the approximate epipolar images of pushbroom satellite stereo imagery based on the PRP in object space, followed by experimental results with accuracy assessment, further discussion, and finally the conclusions.

2. Principles

2.1. Sensor modeling for epipolar resampling

The effective epipolar resampling requires sound geo-locating accuracy of the geometric sensor models, so obtaining high-quality orientation parameters of satellite stereo images is a prerequisite. Today, rigorous geometric sensor modeling of linear array pushbroom satellite imagery is still a challenging task. The calculation of image coordinates based on the rigorous geometric sensor model (i.e., collinearity equations) requires the best scan line search, which adds a considerable amount of computation for stereo mapping and the production of DEMs and digital orthoimage models (DOMs). Besides, vendors of high-resolution commercial satellite images normally provide the end-users with the RPC parameters of the RFM instead of ephemeris and attitude parameters, as well as sensor information. It is demonstrated that the 0.01 pixel high fitting accuracy is totally possible with the 3rd-order form of the RFM, in comparison with the rigorous geometric sensor model (Yang, 2000). Therefore, the RFM can be a good replacement for the rigorous geometric sensor model in the epipolar resampling procedure with satellite stereo imagery. Sometimes the accuracy of the sensor-oriented RFM is not sufficient, and thus additional parameters for bias-compensation (Fraser and Hanley, 2003; Fraser et al., 2006) are calculated using a certain number of GCPs or image tie points in order to ensure a fairly desirable level of geo-positioning accuracy.

2.2. Epipolar geometry of linear pushbroom imagery

The epipolar geometry of traditional frame-based stereo imagery is classically elaborated in many archives of photogrammetry, and it is well known that the parallel epipolar lines can be obtained by projecting the original non-parallel epipolar lines

on a pair of images parallel to the baseline. The generation of such a horizontal image pair, i.e., the epipolar images, is practically identical to digital image rectification. However, in a scene of linear pushbroom satellite imagery, each scan line has its own exterior orientation parameters at the exposure instant; it is difficult to establish the accurate geometric relationship between object space and image space due to the dynamic imaging mode and the highly correlated orientation parameters. According to the PT based epipolar curve definition, suppose p is an image point on the left (right) image, if we project all points on the ray of p to the right (left) image based on the image geometric sensor model, the locus of these projection points, named *ep* here, is thus identified as the epipolar curve of p.

Suppose p is located on an image scanline indexed with i, (l_p, s_p) and $(0, y_p)$ are pixel coordinates and focal plane coordinates of p, respectively, e is the size of sensor detector, y_0 is the translation parameter, then

$$\begin{aligned} i &= l_p \\ y_p &= s_p \times e - y_0. \end{aligned} \tag{1}$$

Let (X_p, Y_p, Z_p) be the coordinates of a certain object point on the ray of p; according to the collinearity conditions, there is

$$\begin{aligned} \begin{pmatrix} X_p \\ Y_p \\ Z_p \end{pmatrix} &= \begin{pmatrix} X_{s_i} \\ Y_{s_i} \\ Z_{s_i} \end{pmatrix} + \lambda_i R_i \begin{pmatrix} 0 \\ y_p \\ -f \end{pmatrix} \\ &= \begin{pmatrix} X_{s_i} \\ Y_{s_i} \\ Z_{s_i} \end{pmatrix} + \lambda_i \begin{pmatrix} r_{i11} & r_{i12} & r_{i13} \\ r_{i21} & r_{i22} & r_{i23} \\ r_{i31} & r_{i32} & r_{i33} \end{pmatrix} \begin{pmatrix} 0 \\ y_p \\ -f \end{pmatrix} \end{aligned} \tag{2}$$

where $(X_{s_i}, Y_{s_i}, Z_{s_i})$ are coordinates of the projection center of the scanline indexed with i, λ_i is the scale factor, f is the focal length, R_i is the rotation matrix of the scanline indexed with i, r_{imn} $(m, n = 1, 2, 3)$ are the elements of R_i.

Then, back-projecting (X_p, Y_p, Z_p) to the right (left) image obtains the image point q. Similarly, suppose q is located on the image scanline indexed with j, $(X_{s_j}, Y_{s_j}, Z_{s_j})$ are coordinates of the projection center, (l_r, s_r) and $(0, y_r)$ are pixel coordinates and focal plane coordinates of q respectively, then

$$\begin{aligned} j &= l_r \\ y_r &= s_r \times e - y_0 \end{aligned} \tag{3}$$

and also

$$\begin{pmatrix} 0 \\ y_r \\ -f \end{pmatrix} = \frac{1}{\lambda_j} R'_j \begin{pmatrix} X_p - X_{s_j} \\ Y_p - Y_{s_j} \\ Z_p - Z_{s_j} \end{pmatrix}, \qquad R'_j = \begin{pmatrix} r_{j11} & r_{j21} & r_{j31} \\ r_{j12} & r_{j22} & r_{j32} \\ r_{j13} & r_{j23} & r_{j33} \end{pmatrix} \tag{4}$$

where λ_j is the scale factor, R'_j is the rotation matrix of the scanline indexed with j, r_{jmn} $(m, n = 1, 2, 3)$ are the elements of R'_j.

When $\lambda_i \approx \lambda_j = \lambda$, combine Eqs. (2) and (4), to obtain

$$\begin{aligned} \begin{pmatrix} 0 \\ y_r \\ -f \end{pmatrix} &= \frac{1}{\lambda_j} R'_j \left(\begin{pmatrix} X_{s_i} - X_{s_j} \\ Y_{s_i} - Y_{s_j} \\ Z_{s_i} - Z_{s_j} \end{pmatrix} + \lambda_i R_i \begin{pmatrix} 0 \\ y_p \\ -f \end{pmatrix} \right) \\ &\approx \frac{1}{\lambda} R'_j \begin{pmatrix} X_{s_i} - X_{s_j} \\ Y_{s_i} - Y_{s_j} \\ Z_{s_i} - Z_{s_j} \end{pmatrix} + R'_j R_i \begin{pmatrix} 0 \\ y_p \\ -f \end{pmatrix}. \end{aligned} \tag{5}$$

Making certain transformations on Eq. (5) gives

$$y_r = -f \frac{r_{j11} A + r_{j21} B + r_{j31} C}{r_{j13} A + r_{j23} B + r_{j33} C} \tag{6}$$

here

$$\lambda = \frac{-r_{j11} \times Xs_{ij} - r_{j11} \times Ys_{ij} - r_{j11} \times Zs_{ij}}{(r_{i12} r_{j11} + r_{i22} r_{j21} + r_{i32} r_{j31}) \times y_p - f(r_{i13} r_{j11} + r_{i23} r_{j21} + r_{i33} r_{j31})}$$

$$\begin{aligned} A &= X_{s_i} - X_{s_j} + \lambda(r_{i12} \times y_p - r_{i13} \times f) \\ B &= Y_{s_i} - Y_{s_j} + \lambda(r_{i22} \times y_p - r_{i23} \times f) \\ C &= Z_{s_i} - Z_{s_j} + \lambda(r_{i32} \times y_p - r_{i33} \times f). \end{aligned}$$

For satellites moving with high stability, the attitude angles of a scene of linear pushbroom imagery are almost constant, and the position of the projection centers can be regarded as a linear function of exposure time or the scanline index, as shown in Eq. (7). Here, $m_1, m_2, m_3, n_1, n_2, n_3$ are the coefficients of one-order polynomials.

$$\begin{aligned} X_{s_j} &= m_1 \times l_r + n_1 \\ Y_{s_j} &= m_2 \times l_r + n_2 \\ Z_{s_j} &= m_3 \times l_r + n_3. \end{aligned} \tag{7}$$

Till then, the mathematical function of epipolar curve *ep* in a simplified form such as Eq. (8) can be derived from Eqs. (3), (6) and (7). Here, k_i $(i = 1, 2, 3, 4)$ are the coefficients that are definitely decided for image point p.

$$k_1 l_r + k_2 s_r + k_3 l_r s_r + k_4 = 0. \tag{8}$$

Apparently, the derived mathematical models of epipolar curves are in a non-linear style and complicated with many orientation parameters included; the shape of the projection trajectory is actually not a straight line; besides, each point on an epipolar curve defined by PT has its specific conjugate epipolar curve, i.e., no conjugate epipolar curves exist theoretically.

Nevertheless, it is indicated that the epipolar curves of linear pushbroom satellite imagery hold two major geometric properties (Habib et al., 2004, 2005). One refers to the **Straightness Approximation**: although the epipolar curves are in a quasi-hyperbola shape at infinity (see Eq. (8)), they are almost straight lines over the extent of stereo image scenes; the other property is **Local Conjugacy**: although the conjugate epipolar curves do not exist in the traditional sense for linear pushbroom stereo images, they can still be considered to exist in a local area or close to the conjugate image points of stereo images by approximation. It is assumed that conjugate image points correspond with each other on these hypothetical conjugate epipolar curves.

2.3. PRP-based epipolarity model

As shown in Fig. 1, *O–XYZ* is the Local Vertical Coordinate system (LVCs), which is a left-handed coordinate system defined on the reference ellipsoid, with the origin point located near the central part of ground cover and with the Y axis tangential to the reference ellipsoid and pointing in the due-north direction. The PRP is defined as the average elevation plane in object space with elevation value H. Suppose p_1 and p_2 are conjugate image points on the left and the right image, respectively, and they are intersected at ground point P. Derived from the PT based epipolar curve definition, ep_1 on the right image indicates the epipolar curve of point p_1, while ep_2 on the left image indicates the epipolar curve of point p_2. Inferred from the orbital stability of the satellite platform and the formerly depicted geometric properties of epipolar curves, ep_1 and ep_2 compose a pair of conjugate epipolar lines by approximation; moreover, if points on ep_1 and ep_2 are projected to the PRP, the projection trajectory will be very close to a straight line named *ED*. Besides, *EP* decided by line *ED* and point P can be regarded as the approximate epipolar plane.

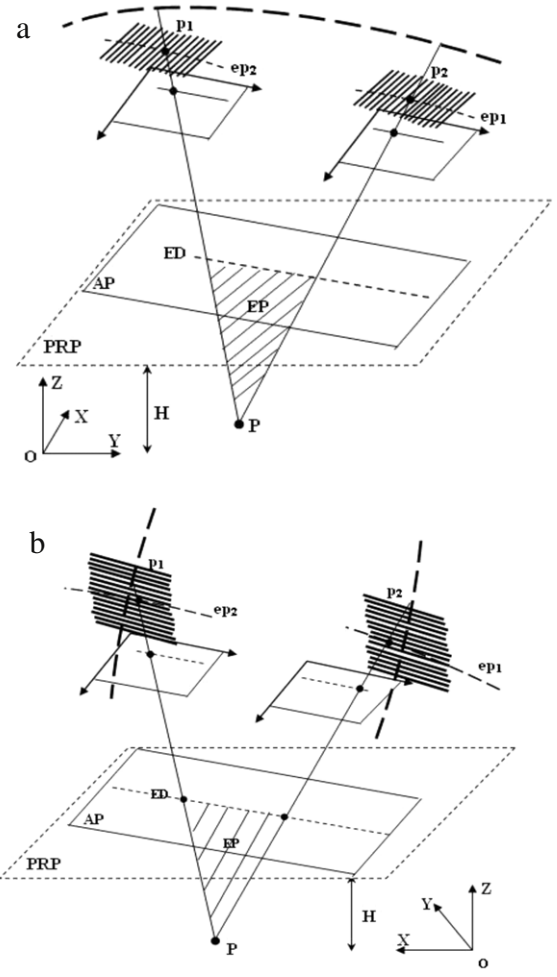

Fig. 1. The PRP-based epipolarity model of satellite stereo imagery. (a) Along-track stereo, and (b) cross-track stereo.

Moreover, it will not be difficult to discover that the PRP projection trajectories of all the conjugate epipolar curves can be approximated as a straight line set parallel with *ED*. To validate our theoretical considerations, coordinate calculation and visual inspection were applied to practical image data in this way: for p_1, select several evenly-distributed sample points from its epipolar curve (i.e., PT), and then calculate the coordinates of their projective points on PRP so as to get the locus; similarly, for p_2, the epipolar curve locus on PRP is also derived. As illustrated in Fig. 2, the horizontal axis and the vertical axis respectively plot the *X* value and the *Y* value of the projective points on PRP in the LVCs. Judging from the line equations fitted and the residuals from these straight lines, it is obvious that for each pair of conjugate epipolar curves, the two loci almost coincide and with a high degree of straightness, while for different pairs of conjugate epipolar curves the loci are almost parallel.

That is to say, the approximate epipolar lines with parallelism can be generated by projecting the original satellite stereo imagery to an image pair parallel to the straight line *ED*, i.e., the equivalent line direction of loci on the PRP for epipolar curves, and thus the PRP-based epipolarity model can be proposed. Actually, the PRP of object space acts as a bridge to build up the pixel coordinate relationships between the original image and the generated epipolar image. Based on such an epipolarity model, it is possible to accomplish the epipolar resampling of satellite stereo imagery in a way that is identical to image digital rectification.

3. PRP-based epipolar resampling

This section describes a new method for epipolar image generation, according to the proposed PRP-based epipolarity model.

It is well known that the essence of the RFM is to associate the geographic coordinates of a ground point with the pixel coordinates of the corresponding image point, where coordinates of both ground point and image point are normalized between −1 and +1 so as to ensure the reliability of the parameter resolving process. The RFM has the following fundamental form:

$$x = \frac{Num_s(U,V,H)}{Den_s(U,V,H)} \qquad y = \frac{Num_L(U,V,H)}{Den_L(U,V,H)} \tag{9}$$

here

$$\begin{aligned} Num_L(U,V,H) &= a_1 + a_2V + a_3U + a_4H + a_5VU \\ &\quad + a_6VH + a_7UH + a_8V^2 + a_9U^2 \\ &\quad + a_{10}H^2 + a_{11}UVH + a_{12}V^3 + a_{13}VU^2 \\ &\quad + a_{14}VH^2 + a_{15}V^2U + a_{16}U^3 + a_{17}UH^2 \\ &\quad + a_{18}V^2H + a_{19}U^2H + a_{20}H^3 \\ Den_L(U,V,H) &= b_1 + b_2V + b_3U + b_4H + b_5VU \\ &\quad + b_6VH + b_7UH + b_8V^2 + b_9U^2 \\ &\quad + b_{10}H^2 + b_{11}UVH + b_{12}V^3 + b_{13}VU^2 \\ &\quad + b_{14}VH^2 + b_{15}V^2U + b_{16}U^3 + b_{17}UH^2 \\ &\quad + b_{18}V^2H + b_{19}U^2H + b_{20}H^3 \\ Num_s(U,V,H) &= c_1 + c_2V + c_3U + c_4H + c_5VU + c_6VH \\ &\quad + c_7UH + c_8V^2 + c_9U^2 \\ &\quad + c_{10}H^2 + c_{11}UVH + c_{12}V^3 + c_{13}VU^2 \\ &\quad + c_{14}VH^2 + c_{15}V^2U + c_{16}U^3 + c_{17}UH^2 \\ &\quad + c_{18}V^2H + c_{19}U^2H + c_{20}H^3 \end{aligned}$$

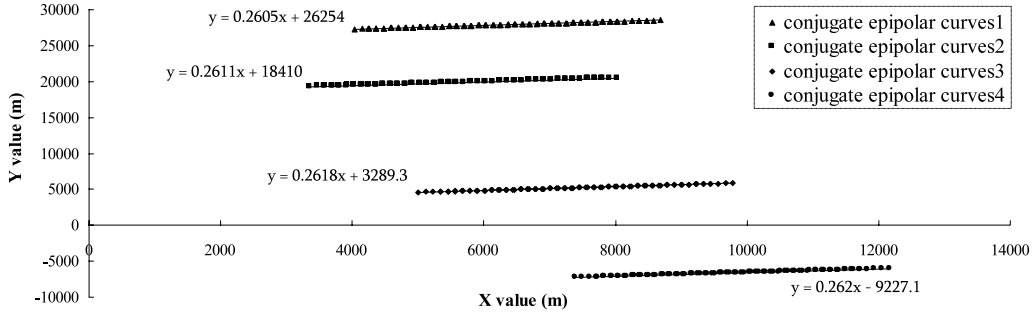

Fig. 2. PRP loci of four pairs of selected conjugate epipolar curves; the residuals from the fitted straight lines are 2e−5, 4e−5, 3e−4 and 5e−5 in meters respectively.

$$\begin{aligned} Den_s(U,V,H) &= d_1 + d_2V + d_3U + d_4H + d_5VU \\ &\quad + d_6VH + d_7UH + d_8V^2 + d_9U^2 \\ &\quad + d_{10}H^2 + d_{11}UVH + d_{12}V^3 + d_{13}VU^2 \\ &\quad + d_{14}VH^2 + d_{15}V^2U + d_{16}U^3 + d_{17}UH^2 \\ &\quad + d_{18}V^2H + d_{19}U^2H + d_{20}H^3 \end{aligned}$$

where a_i, b_i, c_i, d_i are the RPC parameters and $i = 20$; (U, V, H) and (x, y) are the normalized coordinates of ground points and image points, respectively.

Suppose (S, L) are the pixel coordinates of the image point, and $(Lat, Lon, Height)$ are the geodetic coordinates of the corresponding object point, then

$$\begin{aligned} U &= \frac{Lat - Lat\_OFF}{Lat\_SCALE}, \qquad V = \frac{Lon - Lon\_OFF}{Lon\_SCALE}, \\ H &= \frac{Height - H\_OFF}{H\_SCALE}, \\ x &= \frac{S - S\_OFF}{S\_SCALE}, \qquad y = \frac{L - L\_OFF}{L\_SCALE} \end{aligned} \tag{10}$$

where *Lat_OFF*, *Lat_SCALE*, *Lon_OFF*, *Lon_SCALE*, *H_OFF* and *H_SCALE* are the normalized parameters of the ground point coordinates, while *S_OFF*, *S_SCALE*, *L_OFF* and *L_SCALE* are the normalized parameters of the image point coordinates.

To facilitate our description, the coordinate transformation between object space and image space of the stereo imagery is denoted by Eqs. (11)–(14); here, fL and fR are the RFM-based forward coordinate transformation functions of the left and right image scenes, respectively, while fL' and fR' are the RFM-based backward coordinate transformation functions of the left and right image scenes, respectively.

$$(S, L, Height) \xrightarrow{fL} (Lat, Lon) \tag{11}$$

$$(Lat, Lon, Height) \xrightarrow{fL'} (S, L) \tag{12}$$

$$(S, L, Height) \xrightarrow{fR} (Lat, Lon) \tag{13}$$

$$(Lat, Lon, Height) \xrightarrow{fR'} (S, L). \tag{14}$$

In addition, the coordinate transformations between the LVCs coordinates and geodetic coordinates of the object point are denoted by Eqs. (15) and (16); here T and T', respectively, are transformation functions from geodetic coordinates (*Lat, Lon, Height*) to LVCs coordinates (X, Y, Z) and vice versa.

$$(Lat, Lon, Height) \xrightarrow{T} (X, Y, Z) \tag{15}$$

$$(X, Y, Z) \xrightarrow{T'} (Lat, Lon, Height). \tag{16}$$

3.1. Determine line direction of ED

Define PRP as a horizontal plane in the LVCs with average elevation H. As shown in Fig. 3, a is a randomly chosen point on the left image, the ray of which is denoted by R.

Firstly, suppose p_1 and p_2 are two points located on R, respectively above and below the PRP with a height difference of h, then obtain the geodetic coordinates of object points p_1 and p_2 by calculation based on Eq. (11).

Secondly, suppose b and c are the back projective points of p_1 and p_2 on the right image; then obtain their pixel coordinates by calculation based on Eq. (14).

Thirdly, suppose p_3 and p_4 are projective points on the PRP, separately corresponding to the rays of b and c; then obtain the LVCs coordinates of p_3 and p_4 by calculation based on Eqs. (13) and (15). The line connecting p_3 and p_4 thus decides the direction of *ED*, i.e., the direction of approximate epipolar lines on the PRP.

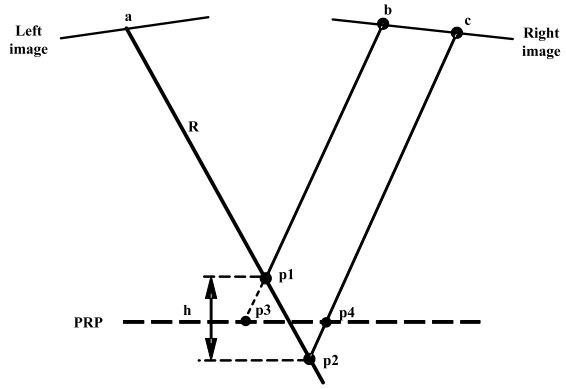

Fig. 3. The decision of approximate line direction of the epipolar curve locus on PRP (strategy with no prior image matching process).

3.2. Determine PRP coverage of epipolar images

Based on Eqs. (11) and (15), coverage of the original left image on the PRP is calculated; similarly, based on Eqs. (13) and (15), PRP coverage of the original right image can also be calculated.

As shown in Fig. 1, AP denotes the PRP coverage of epipolar images, and is decided by the minimum rectangular region enveloping the entire PRP coverage of the original stereo imagery. Here, the horizontal boundary of AP is parallel to the line direction of *ED*, according to the principle of the PRP-based epipolarity model.

3.3. Epipolar resampling

Fig. 4 illustrates how to establish the pixel coordinate relation between the epipolar images and the original stereo imagery, which is the foundation of PRP-based epipolar resampling.

On the one hand, according to the principle of the PRP-based epipolarity model, AP is segmented into grid units with uniform size almost identical with the GSD (Ground Sampling Distance) of the original stereo imagery, and then the grid units of AP are associated with pixels of the left and right epipolar images. It is prescribed that the generated left and right epipolar images have the same PRP coverage as AP, so the left and right epipolar images are of the same size. As shown in Fig. 4, the corresponding relation between planarity coordinates of grid units in the LVCs and pixel coordinates of epipolar images can be established by rotation, translation and scaling transformations.

Suppose O–$X'Y'$ shares the same origin as that of O–XYZ, and with its horizontal axis parallel to the line direction of *ED*. If (X, Y) denote planarity coordinates of grid units in the LVCs, the corresponding coordinates in O–$X'Y'$ can be thus obtained by Eq. (17), where R is the 2D rotation matrix derived from the line direction of *ED* on PRP.

$$\begin{pmatrix} X' \\ Y' \end{pmatrix} = R \times \begin{pmatrix} X \\ Y \end{pmatrix}. \tag{17}$$

Then, suppose (dX', dY') are the translation parameters from the origin of O–$X'Y'$ to the upper left corner of the AP area, g is the grid size, (x_l, y_l) and (x_r, y_r) are pixel coordinates of the left and the right epipolar images, respectively, then

$$\begin{aligned} \begin{pmatrix} x_l \times g \\ y_l \times g \end{pmatrix} &= \begin{pmatrix} X' \\ Y' \end{pmatrix} + \begin{pmatrix} dX' \\ dY' \end{pmatrix} \\ \begin{pmatrix} x_r \times g \\ y_r \times g \end{pmatrix} &= \begin{pmatrix} X' \\ Y' \end{pmatrix} + \begin{pmatrix} dX' \\ dY' \end{pmatrix}. \end{aligned} \tag{18}$$

Obviously, the above rotation, translation and scaling transformations are actually equivalent to Eq. (19), and the left and the

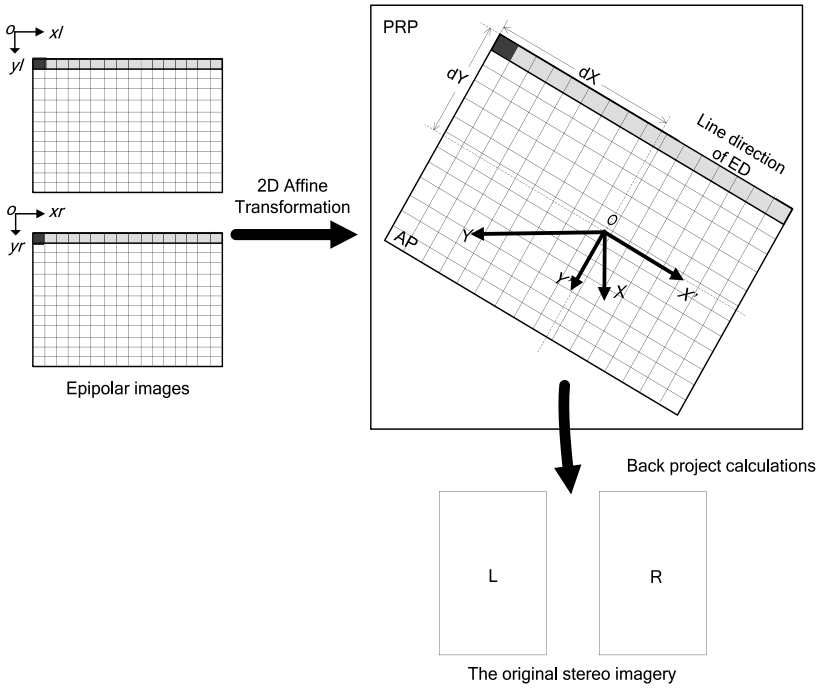

Fig. 4. Coordinate transformation relation of epipolar images and the original stereo imagery.

right epipolar images share the same set of 2D affine transformation parameters $a_0, a_1, a_2, b_0, b_1, b_2$.

$$\begin{cases} X = a_0 + a_1 \times x_r + a_2 \times y_r \\ Y = b_0 + b_1 \times x_r + b_2 \times y_r \end{cases} \quad \begin{cases} X = a_0 + a_1 \times x_l + a_2 \times y_l \\ Y = b_0 + b_1 \times x_l + b_2 \times y_l. \end{cases} \tag{19}$$

On the other hand, for each of the grid units on PRP, the corresponding pixel position on the original left image can be calculated based on Eqs. (12) and (16); similarly, based on Eqs. (14) and (16), the corresponding pixel position on the original right image can also be computed.

Thus, the pixel coordinate relation between the epipolar images and the original stereo imagery is established, by taking the PRP as a bridge. Finally, an appropriate interpolation, e.g., bicubic, is usually performed to finish the entire epipolar resampling process.

4. Experiments and discussion

4.1. Dataset

To prove the theoretical feasibility of the PRP-based epipolarity model and the generality of the developed epipolar resampling approach, 5 m SPOT5-HRG, 1 m IKONOS, 2.5 m IRS-P5, and 0.6 m QuickBird panchromatic stereo images with different imaging constellations and terrain relief were used in this study. Table 1 summarizes the specifications of these four kinds of satellite stereo images.

4.2. Epipolar resampling and accuracy assessment

Before epipolar resampling, bias compensation is performed on the initially provided RPC orientation data in order to achieve a desirable sensor modeling accuracy. In the case of SPOT-HRG stereo imagery in which 21 GCPs are available, we selected half of them as control points to calculate the bias correction parameters of the corresponding RPC orientation data, while the remaining half are used as check points to evaluate the result. In the case of IKONOS stereo imagery in which five control points are available, we used three of them as control points and two as check points to validate the accuracy after the RPC refinement. Since there were no GCPs available for the IRS-P5 and QuickBird images, bias compensation of the RPC orientation parameters was performed based on several pairs of conjugate image points to reach high relative orientation accuracy. The bias compensated RPC parameters of these images all achieved accuracy at the sub-pixel level.

With the refined RPC orientation parameters, the epipolar images of various satellite stereo images were produced. In addition, an ancillary file containing the 2D translation, rotation, and scaling parameters as well as RPC parameters was produced along with each pair of epipolar images. This ancillary file was used to record the pixel coordinate transformation relation between the epipolar images and the original stereo imagery for further utilizations. All the procedures used in the experiment are implemented in the Microsoft Visual C++ Integrated Development Environment on a desktop computer configured with the Microsoft XP Pro operating system.

The generated epipolar stereo models all achieved satisfactory stereoscopic visual effects. Fig. 5(a)–(d) give an overview of stereo anaglyphs of the generated epipolar images; in addition, Fig. 5(e) and (f) show stereo anaglyphs of a local zoomed region in IKONOS stereo imagery with different horizontal parallaxes, and it indicated that points on the roof (see white mark in 5(e)) and on the pavement close by (see white mark in 5(f)) all satisfy the epipolarity constraint.

In order to numerically validate the accuracy of the generated epipolar images, the Leica Photogrammetry Suite (LPS) module of ERDAS IMAGINE software was applied to extract 30 pairs of conjugate image points from each kind of satellite stereo imagery. These conjugate image points are reliable and almost fully distributed over the range of image space. Based on the pixel coordinate relation between the epipolar images and the original stereo imagery, the positions and thus vertical parallaxes

Table 1
Specification of the experimental image datasets.

Stereo imagery	Acquisition date	Image size (pixels)	Terrain type	Mean elevation (m)	GSD (m)	Ground coverage (km)
SPOT5-HRG	2002-08-15 2002-08-18	12,000 × 12,000 12,000 × 12,000	Mountainous, hilly area	370	5	60 × 60 60 × 60
IKONOS	2002-09-07 2002-09-07	19,043 × 7853 19,043 × 7648	Plain	20	1	19 × 8 19 × 8
IRS-P5	2005-01-16 2005-01-16	12,000 × 12,000 12,000 × 12,000	Mountainous, hilly area	100	2.5	30 × 30 30 × 30
QuickBird	2004-03-02 2004-03-02	35,170 × 27,576 35,170 × 23,708	Mountainous, hilly area	600	0.6	21 × 17 21 × 14

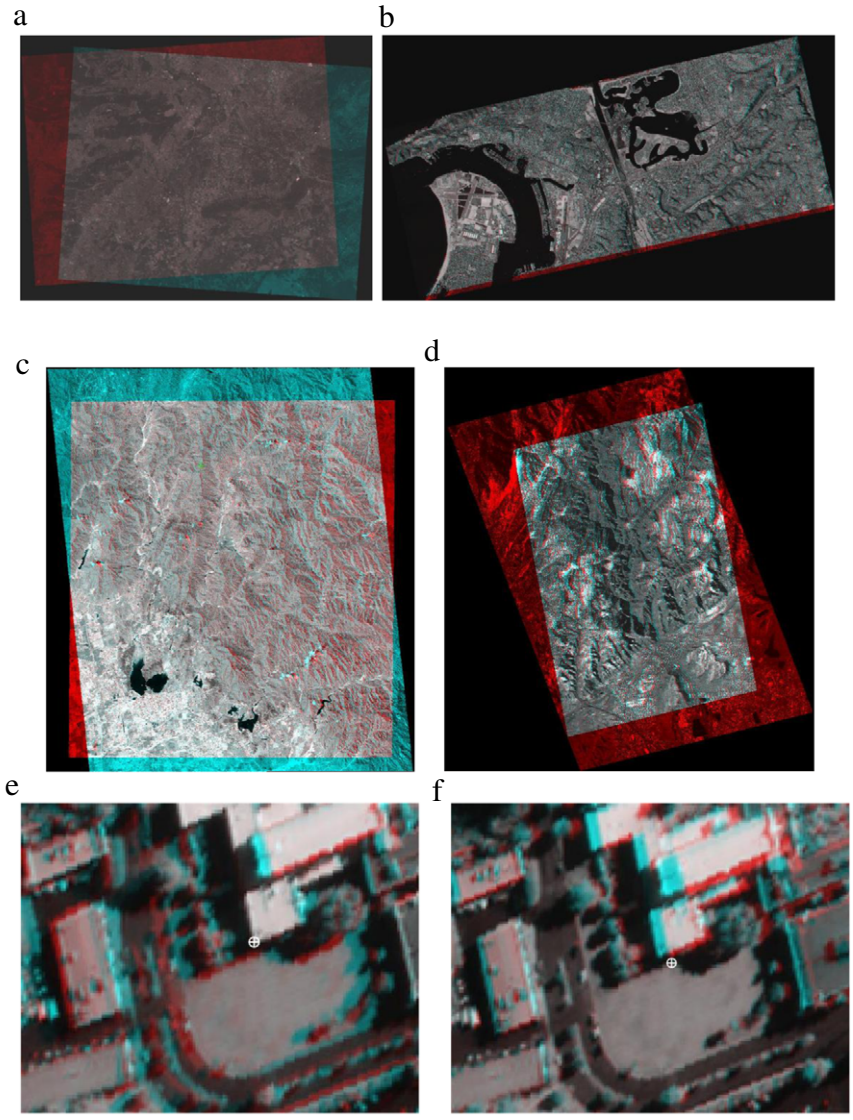

Fig. 5. Stereo anaglyphs of the generated epipolar images.

of these conjugate image points on the generated epipolar images are calculated.

The four line graphs in Fig. 6 respectively show the vertical parallaxes of conjugate image points on the generated SPOT5-HRG, IKONOS, IRS-P5, and QuickBird epipolar images, where the horizontal axis shows the index of conjugate image points ordered by increasing parallax, while the vertical axis shows the value of vertical parallax.

Moreover, Table 2 gives the statistics where Q_{Min}, Q_{Max}, Q_{Mean} and Q_{RMS} indicate minimum, maximum, mean and root mean square values of vertical parallaxes, respectively.

Table 2
Vertical parallax statistics of conjugate image points on generated epipolar images (unit: pixel).

Stereo imagery	Q_{Min}	Q_{Max}	Q_{Mean}	Q_{RMS}
SPOT5-HRG	−0.480	0.250	−0.197	0.185
IKONOS	−0.638	0.427	0.003	0.248
IRS-P5	−0.575	0.397	−0.016	0.231
QuickBird	−0.779	0.666	−0.050	0.311

Judging from the results indicated by Fig. 6 and Table 2, the vertical parallaxes all reach sub-pixel level. It is clear that when the

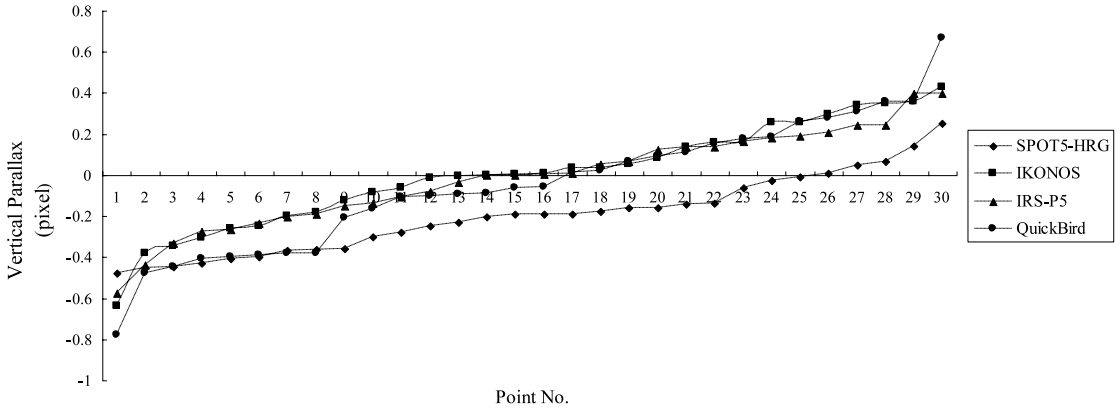

Fig. 6. Vertical parallaxes of conjugate image points on the generated epipolar images.

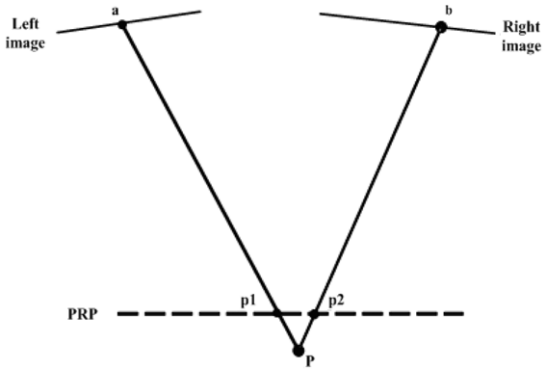

Fig. 7. Deciding the approximate line direction of the epipolar curve locus on PRP (strategy with prior image matching process).

accuracy of image orientation data is satisfactory, the comparable rigorous satellite epipolar images with subtle vertical parallax can be generated by the proposed epipolar resampling method.

Through repetitive tests, we also find that when the value of parameter h in Fig. 3 is replaced with different values (e.g., ranging from 20 to 400 m), each time the vertical parallaxes of conjugate image points are almost the same, with variations in Q_{RMS} being smaller than 1×10^{-2} pixel. That is to say, the value of h has little effect on the quality of epipolar resampling and thus can be chosen flexibly in practice.

Experiments also indicate that such an epipolar resampling method is also feasible with long-strip satellite stereo imagery. Generally speaking, the terrain relief has no effect on such a method, since the four kinds of satellite images used in our experiment actually cover various terrain types such as flat, hilly, and mountainous areas. Overall, it is the accuracy of the image orientation data that primarily affects the quality of the epipolar resampling result.

4.3. Further discussion

It is noted that the direction of ED can be additionally determined by any pair of conjugate image points. As shown in Fig. 7, p_1 and p_2 are the projection points of a pair of conjugate image points represented by $\boldsymbol{a}$ and $\boldsymbol{b}$. The direction of the line connecting p_1 and p_2 can be identified as the approximate arranging direction of epipolar lines on the PRP.

In this way, we successively use each pair of conjugate image points to determine the epipolar arranging direction, and then calculate the average and RMS values of the vertical parallaxes. The results listed in Table 3 indicate that it can serve as another strategy to decide the approximate line direction of the epipolar curve locus on the PRP, i.e., from just one pair of reliably-matched conjugate image points and the high-accuracy PRC parameters. However, when the pair of conjugate image points used here happens to intersect an object point on or quite near the PRP, unstable or incorrect results will be derived. Therefore, with regard to the procedure's simplicity and reliability, it is recommended that the former depicted strategy (see Fig. 3) without a prior image matching process be adopted in practice.

Table 3
Vertical parallax statistics of conjugate image points on generated epipolar images (unit: pixel).

Point no.	SPOT5-HRG		IKONOS		IRS-P5		QuickBird	
	Q_{Mean}	Q_{RMS}	Q_{Mean}	Q_{RMS}	Q_{Mean}	Q_{RMS}	Q_{Mean}	Q_{RMS}
1	−0.038	0.222	−0.003	0.252	0.012	0.221	0.014	0.369
2	0.264	0.261	0.019	0.242	0.256	0.245	0.064	0.401
3	0.093	0.237	0.009	0.244	−0.138	0.225	0.048	0.391
4	0.154	0.245	−0.006	0.254	−0.124	0.224	−0.035	0.343
5	0.206	0.252	0.004	0.247	0.117	0.227	−0.127	0.309
6	−0.022	0.223	0.002	0.248	0.048	0.222	−0.063	0.330
7	0.227	0.255	0.001	0.249	−0.205	0.232	−0.182	0.301
8	0.457	0.289	−0.009	0.258	−0.119	0.224	−0.069	0.328
9	0.494	0.295	−0.011	0.259	0.461	0.289	−0.096	0.317
10	−0.178	0.207	−0.033	0.287	0.152	0.231	−0.098	0.317
11	−0.007	0.225	0.002	0.248	−0.003	0.221	−0.142	0.306
12	0.243	0.258	0.001	0.249	−0.328	0.251	−0.174	0.302
13	0.165	0.247	0.033	0.243	0.124	0.228	0.116	0.438
14	−0.209	0.204	0.001	0.249	−0.185	0.230	0.034	0.382
15	0.086	0.236	0.027	0.242	−0.328	0.251	−0.077	0.324
16	0.117	0.241	0.007	0.245	0.008	0.221	0.009	0.366
17	−0.063	0.219	−0.023	0.273	0.134	0.229	−0.085	0.321
18	−0.177	0.207	−0.018	0.267	−0.048	0.221	−0.052	0.335
19	−0.196	0.205	0.019	0.242	0.096	0.225	−0.188	0.301
20	−0.051	0.220	−0.014	0.263	0.476	0.293	0.017	0.371
21	0.592	0.311	−0.008	0.256	0.444	0.285	−0.018	0.351
22	−0.406	0.189	0.015	0.243	−0.111	0.223	0.033	0.381
23	−0.257	0.200	0.004	0.247	0.177	0.234	−0.080	0.323
24	−0.055	0.220	0.020	0.242	−0.036	0.221	−0.119	0.311
25	0.050	0.232	0.016	0.242	0.077	0.224	0.133	0.451
26	−0.324	0.195	0.044	0.249	−0.144	0.226	−0.267	0.310
27	−0.240	0.201	−0.018	0.267	−0.248	0.238	−0.061	0.331
28	0.172	0.248	0.022	0.241	−0.173	0.228	−0.267	0.310
29	−0.096	0.215	−0.023	0.274	0.008	0.221	−0.210	0.301
30	−0.046	0.221	−0.021	0.270	−0.215	0.233	−0.176	0.301

5. Conclusions

This paper extends our previous work on the epipolarity model for satellite stereo imagery based on the PRP in object space. We have presented a PRP-based epipolar resampling method for generating approximate epipolar images from linear pushbroom satellite images acquired either in the along-track or cross-track mode. SPOT5-HRG, IKONOS, IRS-P5, and QuickBird stereo images

have been used to quantitatively evaluate the proposed method. The experimental results demonstrate that our method works well on both along-track and cross-track linear pushbroom satellite stereo images with different stereoscopic viewing modes, spatial resolution, and terrain conditions. Our study also indicates that the accuracy of image orientation data generally determines the correctness of the epipolar resampling process.

In conclusion, the Approximated Straightness and Local Conjugacy properties of epipolar curves within the satellite image region provide important information on the proposition of our PRP-based epipolarity model. Also the successful use of this model for epipolar image generation again proves the practical applicability of these properties and provides experience for further research. Based on this model, the relationship of the pixel coordinates between the original image and the generated epipolar image can be directly established by geometric sensor model (or RFM) based computation, without prior sensor model transformation or image matching performances being needed. Moreover, by arranging the approximate epipolar lines on the defined PRP, the stereoscopic model that is parallel to the object space can be acquired with a consistent resolution. This helps to ensure an impressive and sound stereo-viewing effect. Overall, the PRP-based epipolar resampling method is simple, reliable, and applicable. So far, it has been successfully applied to the stereo mapping and automated DEM generation software modules of linear pushbroom satellite images developed at the State Key Laboratory for Information Engineering in Surveying, Mapping & Remote Sensing (LIESMARS) at Wuhan University in China.

Acknowledgements

This work was supported by the National High Technology Research and Development Program (2009AA12Z120) and the National Natural Science Foundation of China (40901209). It was also funded by Key Laboratory of Geo-informatics of State Bureau of Surveying and Mapping (No. 200902). The authors would like to thank the anonymous reviewers for their valuable comments.

References

Alrousan, N., Cheng, P., Petrie, G., Toutin, T., Zoej, M.J.V., 1997. Automated DEM extraction and orthoimage generation from SPOT level 1B imagery. Photogrammetric Engineering and Remote Sensing 63 (8), 965–974.

Bang, K.I., Jeong, J.S., Kim, K., Cho, W., 2003. Automatic DEM generation using IKONOS stereo imagery. In: Proc. 2003 IEEE International Geoscience and Remote Sensing Symposium, IGARSS'03, Toulouse, France, 21–25 July, vol. 7, pp. 4289–4291.

Cochran, S.D., 1995. Adaptive vergence for the stereo matching of oblique imagery. ISPRS Journal of Photogrammetry and Remote Sensing 50 (4), 21–28.

Fraser, C.S., Dial, G., Grodecki, J., 2006. Sensor orientation via RPCs. ISPRS Journal of Photogrammetry and Remote Sensing 60 (3), 182–194.

Fraser, C.S., Hanley, H.B., 2003. Bias compensation in rational functions for IKONOS satellite imagery. Photogrammetric Engineering and Remote Sensing 69 (1), 53–57.

Fraser, C.S., Yamakawa, T., 2004. Insights into the affine model for high-resolution satellite sensor orientation. ISPRS Journal of Photogrammetry and Remote Sensing 58 (5–6), 275–288.

Habib, A.F., Kim, E.M., Morgan, M., Couloigner, I., 2004. DEM generation from high resolution satellite imagery using parallel projection model. International Archives of the Photogrammetry, Remote Sensing and Spatial Information Sciences 35, (Part B1), 393–398.

Habib, A.F., Morgan, M., Jeong, S., Kim, K., 2005. Epipolar geometry of line cameras moving with constant velocity and attitude. Electronics and Telecommunications Research Institute Journal 27 (2), 172–180.

Hashimoto, T., 2000. DEM generation from stereo AVNIR images. Advances in Space Research 25 (5), 931–936.

Hu, F., Wang, M., Li, D., 2008. A novel epipolarity model of satellite stereo-imagery based on virtual horizontal plane of object-space. In: Proc. International Conference on Earth Observation Data Processing and Analysis. ICEODPA, Wuhan, China, 28–30 December. In: SPIE, vol. 7285, 72851D. 8p.

Jaehong, O.H., Shin, S.W., Kim, K., 2006. Direct epipolar image generation from IKONOS stereo imagery based on RPC and parallel projection model. Korean Journal of Remote Sensing 22 (5), 451–456.

Kim, T., 2000. A study on the epipolarity of linear pushbroom images. Photogrammetric Engineering and Remote Sensing 66 (8), 961–966.

Kornus, W., Alamús, R., Ruiz, A., Talaya, J., 2006. DEM generation from SPOT-5 3-fold along track stereoscopic imagery using autocalibration. ISPRS Journal of Photogrammetry and Remote Sensing 60 (3), 147–159.

Lee, H.Y., Kim, T., Park, W., Lee, H.K., 2003. Extraction of digital elevation models from satellite stereo images through stereo matching based on epipolarity and scene geometry. Image and Vision Computing 21 (9), 789–796.

Lee, H.Y., Park, W., 2002. A new epipolarity model based on the simplified pushbroom sensor model. In: International Achieves of the Photogrammetry, Remote Sensing and Spatial Information Sciences, IAPRS & SIS, Proc. the ISPRS Commission IV Symposium on Geospatial Theory, Processing and Appilications, Ottawa, Canada, 9–12 July. 34 (Part 4), pp. 631–636.

Morgan, M., 2004. Epipolar Resampling of Linear Array Scanner Scenes. Ph.D. Dissertation, University of Calgary, Canada, 187p.

Morgan, M., Kim, K., Jeong, S., Habib, A., 2004a. Indirect epipolar resampling of scenes using parallel projection modeling of linear array scanners. International Archives of the Photogrammetry, Remote Sensing and Spatial Information Sciences 35, (Part B3), 508–513.

Morgan, M., Kim, K., Jeong, S., Habib, A., 2004b. Epipolar geometry of linear array scanners moving with constant velocity and constant attitude. International Archives of the Photogrammetry, Remote Sensing and Spatial Information Sciences 35, (Part B3), 52–57.

Morgan, M., Kim, K., Jeong, S., Habib, A., 2006. Epipolar resampling of space-borne linear array scanner scenes using parallel projection. Photogrammetric Engineering and Remote Sensing 72 (11), 1255–1263.

Ono, T., Honmachi, Y., Ku, S., 1999. Epipolar resampling of high resolution satellite imagery. In: Proc. Joint Workshop of ISPRS WG I/1, I/3 and IV/4 Sensors and Mapping from Space, Hannover, Germany, 27–30 September. 7 p (on CDROM).

Su, J.Y., 2002. Study of SPOT epipolar image polynomial fitting based on matching constraint. Remote Sensing Information 0 (4), 11–14.

Torr, P.H.S., 2002. Bayesian model estimation and selection for epipolar geometry and generic manifold fitting. International Journal of Computer Vision 50 (1), 35–61.

Wolf, P.R., Dewitt, B.A., 2000. Elements of Photogrammetry with Applications in GIS, 3/e. McGraw-Hill, Toronto, 608p.

Yang, X.H., 2000. Accuracy of rational function approximation in photogrammetry. International Archives of Photogrammetry and Remote Sensing 33, (Part B3), 146–156.

Zhang, Z.Y., 1998. Determining epipolar geometry and its uncertainty: a review. International Journal of Computer Vision 27 (2), 161–195.

Zhao, D., Yuan, X.X., Liu, X., 2008. Epipolar line generation from IKONOS imagery based on rational function model. International Archives of the Photogrammetry, Remote Sensing and Spatial Information Sciences 37, (Part B4), 1293–1297.